CHEMNANOMAT

CHEMISTRY OF NANOMATERIALS FOR ENERGY, BIOLOGY AND MORE

www.chemnanomat.org

Accepted Article

Title: Ionothermal Synthesis of Carbon/TiO2 Nanocomposite for Supercapacitor

Authors: Runming Tao, Tao Wang, Juntian Fan, Harry M. Meyer III, Albina Y. Borisevich, Chi-Linh Do-Thanh, and Sheng Dai

To be cited as: *ChemNanoMat* **2022**, e202200075

Link to VoR: https://doi.org/10.1002/cnma.202200075

A Journal of

ACES Asian Chemical Editorial Society

A sister journal of **Chemistry – An Asian Journal** and **Asian Journal of Organic Chemistry**

WILEY-VCH

10.1002/cnma.202200075

WILEY-VCH

RESEARCH ARTICLE

Ionothermal Synthesis of Carbon/TiO_2 Nanocomposite for Supercapacitor

Runming Tao,[abc] Tao Wang,*[b] Juntian Fan, [a] Harry M. Meyer III,[d] Albina Y. Borisevich,[d] Chi-Linh Do-Thanh,[a] Sheng Dai *[ab]

[a] Dr. R. Tao, J. Fan, Dr. C.-L. Do-Thanh, Prof. S. Dai
Department of Chemistry
The University of Tennessee
Knoxville, Tennessee 37996, USA
E-mail: dais@ornl.gov
[b] Dr. T. Wang, Prof. S. Dai
Chemical Sciences Division
Oak Ridge National Laboratory
Oak Ridge, Tennessee 37830, USA
E-mail: wangtaojluchem@gmail.com
[c] Dr. R. Tao
Electrification and Energy Infrastructures Division
Oak Ridge National Laboratory
Oak Ridge, Tennessee 37831, USA
[d] Dr. H. M. Meyer III, Dr. A. Y. Borisevich
Center for Nanophase Materials Sciences
Oak Ridge National Laboratory
Oak Ridge, Tennessee 37831, USA

Supporting information for this article is given via a link at the end of the document.

Abstract: A facile *in-situ* ionothermal strategy is designed to synthesize carbon/oxide composites with nanoporous structure. Ionic liquids play key roles in this ionothermal method as the solvents, porous structure directing templates and carbon sources. The interaction between ionic liquids and oxides greatly improves the carbon yield of ionic liquids from nearly 0 to 18 wt.%. With the synergistic effects of the high electrical conductivity of the nitrogen-rich carbon species and the Ti^{3+} self-doping enhanced electrical conductivity of TiO_2, C/TiO_2-4 composite exhibits better electrochemical performance than C/SiO_2 and C/Nb_2O_5 do as a supercapacitor electrode material, delivering a high specific capacitance of 152.4 F g^{-1} at 5 mV s^{-1} with good capacitance retentions of 84.7%, 72.2% and 46.0% at 30, 100 and 500 mV s^{-1}, respectively.

Introduction

To resolve the current environmental and energy crises, high-performance energy storage devices are urgently needed.[1] Supercapacitors with the large surface area of the porous electrode materials together with faradic reactions delivering high energy and power densities are thereby considered to be promising candidates for alternating the conventional dielectric capacitors.[2] Owing to the accessible porosity, chemical stability and ideal capacitive behavior, TiO_2 is a promising electrode material for supercapacitors.[3] However, TiO_2 with a wide bandgap of 3.2 eV and poor electrical conductivity can dramatically restrict the high-rate performance of supercapacitors.[4] To realize the application of TiO_2 as electrode material for supercapacitors, scientists recently proposed that carbon (C) / TiO_2 composites can be effective electrode materials,[5] due to their excellent compatibility, including accessible surface, good chemical stability and electric double-layer storage mechanism.[3a, 3b, 6] Most importantly, carbon materials with superb electrical conductivity effectively desirably compensate the low electrical conductivity of TiO_2 materials and thus ensure the rate-capability of the supercapacitors.[4b, 5a] Thereby, to develop high-performance supercapacitors, a facile preparation strategy of high-performance C/TiO_2 composites is of interest.

Ionic liquids (ILs) refer to the liquid-state semi-organic salts at below 100 °C.[7] Owing to their promising properties, namely the negligible vapor pressure with the solvating versatility and excellent thermal stability, which are mainly due to the strong Coulombic interactions between their constituent ions induced high ionicity,[8] ILs exhibit promising potential in many fields, including the applications of syntheses (solvent and/or template), separation and energy storage devices.[9] Noticeably, our group priorly extended the use of ILs as an effective carbon source to produce highly porous carbon materials and as porous structure directing templates to syntheses porous transition metal compounds since 1999.[9a, 9b, 10] Inspired by the prior work, we propose an facile in-situ ionothermal synthesis strategy for the preparation of carbon/transition metal oxide nanoporous composite materials, which concurrently uses ILs as the solvents, templates and carbon sources.

10.1002/cnma.202200075

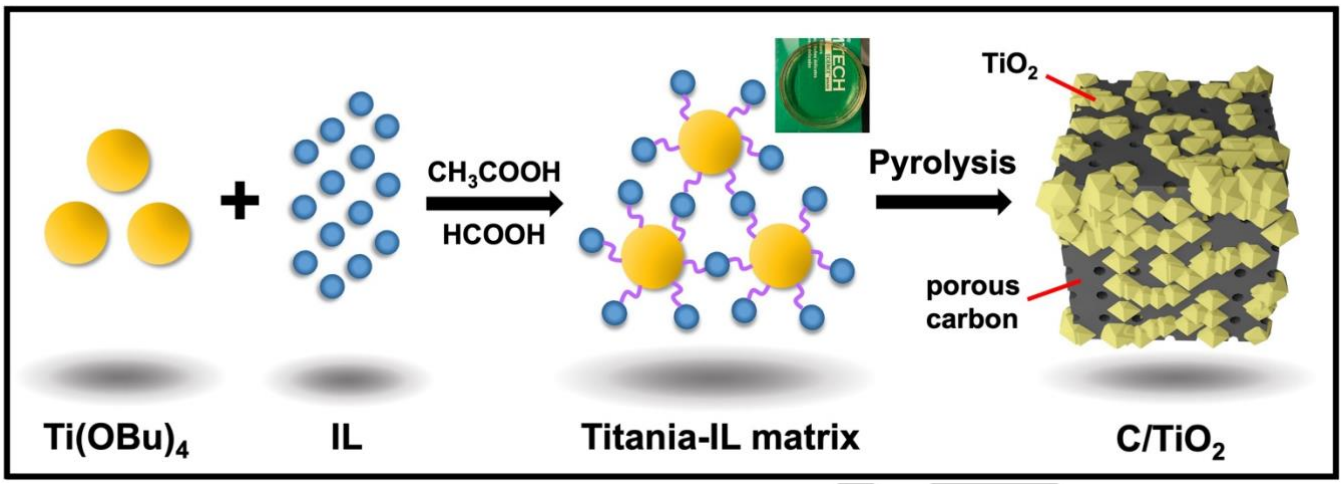

Scheme 1. Scheme of the ionothermal synthesis of C/TiO_2 composite (the purple curved line of the titania-IL matrix represents the hydrogen bonding between IL and titania species *via* nonhydrolytic sol–gel process).

Herein, as the scheme shown in Scheme 1, a series of carbon/oxides (C/TiO_2, C/SiO_2, and C/Nb_2O_5) composites with nanoporous feature is facilely prepared through an in-situ ionothermal synthesis strategy. Typically, the preparation of C/TiO_2 composite involves a nonhydrolytic sol-gel process of the mixture of IL and titanium (IV) butoxide ($Ti(OBu)_4$) to form titania-IL matrix *via* electrostatic interaction and hydrogen bonding followed by a high-temperature pyrolysis treatment, which applies formic acid and acetic acid as the oxygen donors and ensures the uniform hydrolysis and the following poly-condensation.[10b, 11] In this ionothermal synthesis strategy, the ILs are not only applied as the solvents, but also are employed as the porous structure directing templates and carbon sources. Noticeably, this approach not only exhibits desirable porosity (including micropores and mesopores) and promising versatility, but also utilizes the reduction effect of IL pyrolysis to achieve self-doping for further mediating the poor electrical conductivity of TiO_2. Moreover, the interaction between IL and TiO_2 ensures the high carbon yield of IL. Thereby, C/TiO_2-4 composite delivers improved electrochemical performance compared to C/SiO_2 and C/Nb_2O_5 as a supercapacitor electrode material, benefited from the synergistic effects of the Ti^{3+} self-doping enhanced electrical conductivity of TiO_2 and the high electrical conductivity of the nitrogen-rich carbon.

Results and Discussion

As shown in Figure 1a, the X-ray diffraction (XRD) pattern of the obtained C/TiO_2-4 composite conforms to the standard diffraction pattern (ICDD 01-070-6826), suggesting that the formed TiO_2 is anatase-phased, which belongs to the tetragonal system with a space group of $I4_1/amd$). As expected, the typical board diffraction peak of the amorphous C is observed at around 25 °, indicating the successful formation of carbon from IL during the spatially confined pyrolysis of IL. Moreover, the XRD Rietveld refinement (Figure 1b) suggests the existence of the amorphous C and reveals that the anatase TiO_2 has lattice parameters of a = b = 3.792 Å, c = 9.489 Å and $\alpha = \beta = \gamma = 90$ ° with a unit cell volume of 136.4 $Å^3$. Compared to the lattice information of the standard anatase TiO_2 (a = b = 3.771 Å, c = 9.430 Å and $\alpha = \beta = \gamma = 90$ ° with a unit cell volume of 134.1 $Å^3$),[12] the enlarged lattice of the obtained anatase TiO_2 material may be attributed to the reduction of Ti^{4+} to Ti^{3+} during the high-temperature pyrolysis (Ti^{4+} to Ti^{3+} have ionic radii of 74.5 and 81 pm, respectively).[13] Furthermore, according to the Scherrer equation, the grain size of the formed TiO_2 is estimated to be 13.1 nm.

10.1002/cnma.202200075

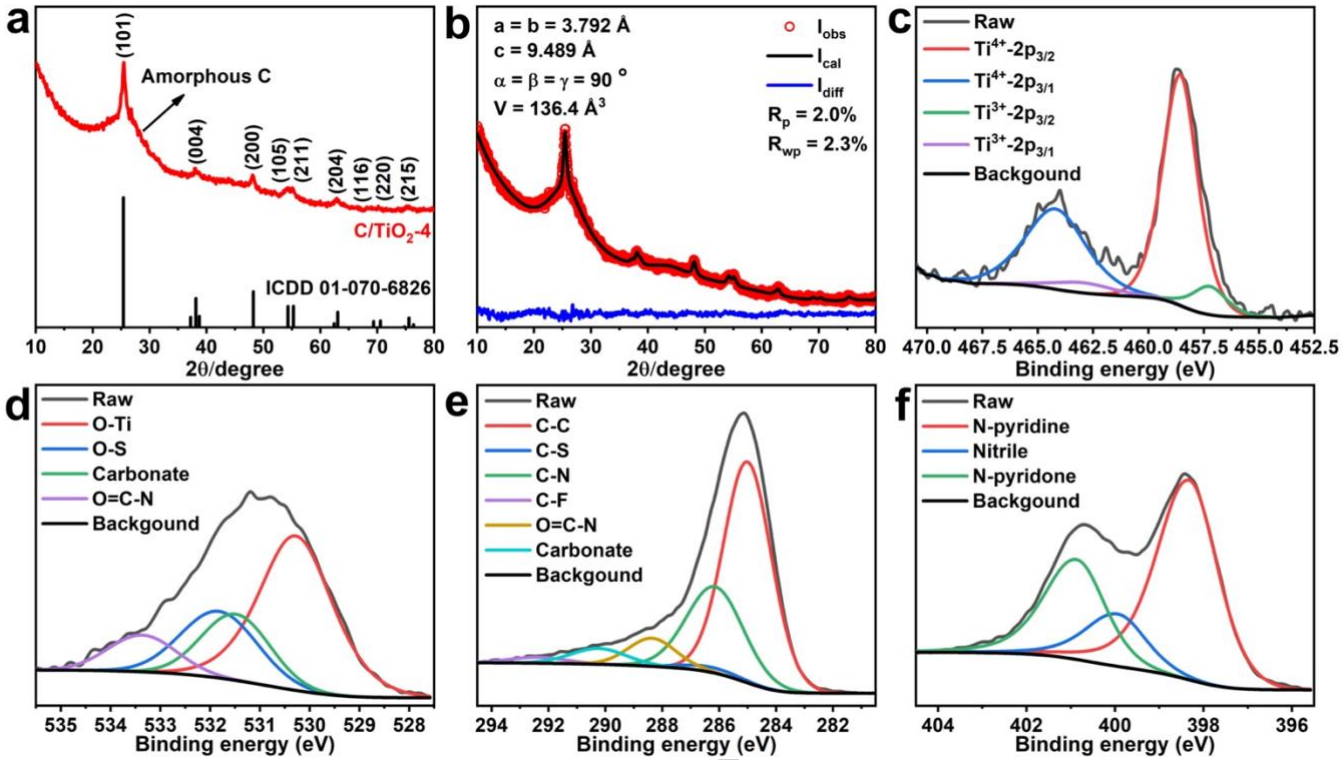

Figure 1. a and b). XRD pattern and its corresponding Rietveld refinement of C/TiO_2-4. c-f). HRXPS spectra of C/TiO_2-4 for Ti, O, C and N.

As a complement to XRD, Fourier-transform infrared spectroscopy (FTIR) and Raman spectroscopy were further applied. The FTIR spectrum is presented in Figure S1. The bands at wavenumbers of 3297, 2256 and 1638 cm^{-1} are assigned to the vibrational modes of N–H, C≡N and C=N bonds, which may imply the formation of N-rich C species in the composite.[14] Noticeably, the contained lone pair of electrons on N can probably act as the Lewis bases to interact with the cations from the electrolytes and to benefit the electrochemical energy storage performance.[15] As shown in Figure S2, the obvious E_g^* mode at around 144 cm^{-1} reveals the anatase-phased feature of the as-formed TiO_2 nanocrystals with long-range order.[16] Additionally, as displayed in Figure S3, the large peak at 1350 cm^{-1} is attributed to the D band due to the defects and the disordered portions of sp^3-coordination of the amorphous C species, and the sharp peak at 1590 cm^{-1} is ascribed to the G band of the graphite-like C.[17] After Gaussian-based deconvolution, the relative area ratio-related I_G/I_D value is about 0.4, which suggests that the obtained C material has a low graphitization-degree with relatively high electrical conductivity and abundant defects, benefitting the electron and mass transfers kinetics in electrochemical application.[18]

To study the potential reduction effect of the pyrolysis and the formed C species, X-ray photoelectron spectroscopy (XPS) analysis was conducted. The broad XPS spectrum of C/TiO_2-4 in Figure S4, indicates the existences of Ti-3p, O-1s, N-1s and C-1s elements. As the high-resolution XPS (HRXPS) spectrum of Ti-2p displayed in Figure 1c, besides the Ti^{4+}-$2p_{3/2}$ and Ti^{4+}-$2p_{1/2}$ peaks at 458.6 and 464.3 eV, correspondingly,[19] the two additional small peaks can be observed at 457.3 and 463.4 eV, which are rooted from the Ti^{3+}-$2p_{3/2}$ and Ti^{3+}-$2p_{1/2}$, respectively.[20] Additionally, the HRXPS study reveals that 11 at.% of Ti^{3+} appears in the TiO_2 material. Such observation above uncovers that the reduction effect indeed exists during the pyrolysis. Interestingly, the apparent Ti^{3+} cations may act as the p-typed self-dopant to cooperate with the formed C and thereby to further synergistically enhance the electrical conductivity of the prepared materials to improve the electrochemical performance.[4b, 20-21] As shown in Figure 1d, the main peak of O-1s is located at 530.3 eV, which is mainly due to the oxygen species of TiO_2.[22] The tiny peaks at 531.5, 531.8 and 533.4 eV are attributed to the carbonate species, O-S and O=C-N bonds from the sample.[4b, 19b, 23] The C-1s HRXPS spectrum in Figure 1e, has a primary peak at 285.0 with five small peaks centered at 285.0, 286.1, 286.3, 288.4, 292.4 and 290.2 eV, corresponding to the C-C, O=C-N, C-S, C-O, C-F bonds and carbonate species, respectively.[4b, 24] Noticeably, the C-C bond is ascribed to the formed C from IL pyrolysis, and those carbon-oxygen/nitrogen/fluorine/sulfur species can result in the abundant defects of the porous C,[9a] which are in good agreement with the Raman spectroscopy results (Figure S3). As presented in Figure 1f, the N-1s HRXPS spectrum exhibits three peaks located at 398.3, 399.9 and 400.9 eV, assigning to pyridine, nitrile and pyridine species, respectively.[25]

10.1002/cnma.202200075

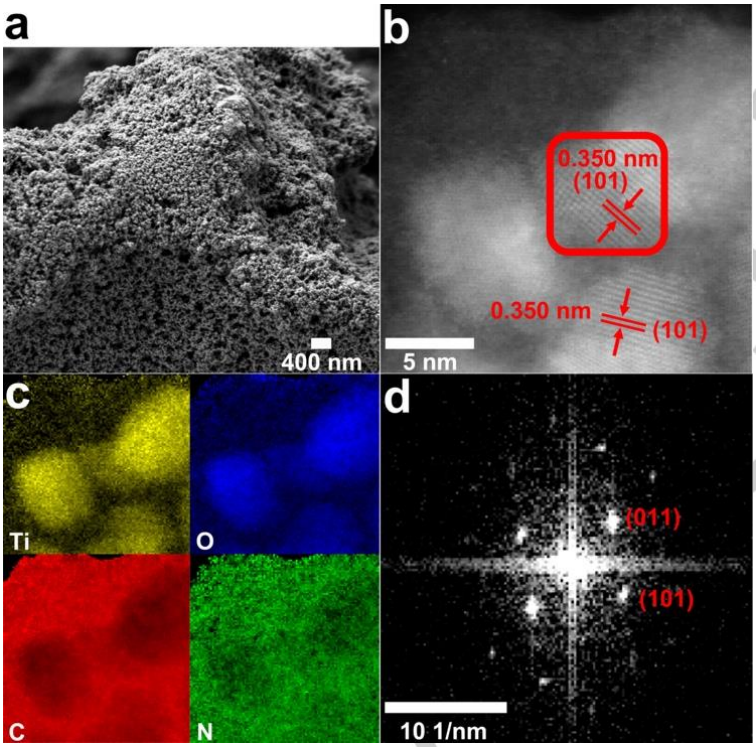

Figure 2. a-c). SEM, TEM and EELS elemental mapping images of C/TiO_2-4, respectively. d). The FFT diffractogram pattern from an image (Figure S8b) of the same TiO_2 crystallite as defined by the red box on b).

To characterize the microstructure of the composites, nitrogen adsorption study was performed. As shown in Figure S5, the Brunauer-Emmett-Teller (BET) specific surface area of C/TiO_2-4 is as high as 409.0 m^2 g^{-1}. The corresponding Barrett-Joyner-Halenda (BJH) pore size distribution plot reveals the existence of micropores and mesopores (Figure S6). To further study the morphology of C/TiO_2-4 composite, scanning electron microscope (SEM) and transmission electron microscope (TEM) were applied. As the SEM image displayed in Figure 2a, C/TiO_2-4 exhibits a typical three-dimensional porous structure composed of the agglomerated C and TiO_2 nanoparticles, being consistent with the aforementioned results of the nitrogen adsorption test. The SEM energy-dispersive X-ray (EDX) spectroscopy elemental mapping images in Figure S7 reveals that the Ti, O, N and C elements are homogenously distributed on the composite. Furthermore, the TEM image in Figure 2b suggests that the average crystallite size of TiO_2 is around 11 nm, which is close to the crystallite size estimated from XRD and may potentially benefits the electrochemical kinetics in energy storage applications. Moreover, the estimated lattice fringe of TiO_2 in the HRTEM image is about 0.350 nm, corresponding to the (101) crystallographic plane of the anatase-phased TiO_2. Noticeably, as shown in Figure S8, no lattice fringe can be observed on the obtained C species (the red color marked area), which indicates the amorphous feature of the formed C species, sharing coherence with the results of XRD, Raman and selected area electron diffraction (SAED) pattern. To further study the distribution of elements, TEM EELS elemental mapping was performed. As displayed in Figure 2c, Ti and O elements are evenly distributed on the TiO_2 nanocrystallites. N shares highly overlapped regions with C, confirming the successful formation of N-rich carbon species, which may act as Lewis bases to interreact with the cations from the electrolytes and thereby enhance the electrochemical energy storage performance, due the abundant lone pair of electrons on N.[15] Such TEM electron energy loss spectroscopy (EELS) elemental mapping results are consistent with the observation from FTIR and XPS above. Moreover, the fast Fourier transform (FFT) diffractogram patterns in Figure 2d and Figure S9 indicate the single-crystalline property of the formed TiO_2 nanocrystallite and the amorphous feature of the prepared C material, respectively.

Furthermore, a thermogravimetric analysis (TGA) was performed to study the C composition in the C/TiO_2-4 material. As shown in Figure S10 a, the initial weight loss at below 100 °C can be ascribed to the removal of moisture in the sample. From around 380 to 550 °C, the obvious weight loss is assigned to the burning of C species, which suggests that the C composition is around 64.4 wt.%, demonstrating the high C yield of the proposed ionothermal synthesis strategy. This is attributed to the promising spatially confined pyrolysis of titania-IL matrix because the pure [BMIm][NTf_2] IL without nitrile group fails to produce C species (Figure S10 b). Noticeably, the more IL is used, the higher weight loss can be observed (Figure S10a). This reflects an increase of carbon yield. Additionally, as displayed in Figure S12 a, it's interesting to note that even at a high composition of TiO_2, the measured specific surface areas of C/TiO_2 composites are still close to 200 m^2 g^{-1}, corresponding to the nanoporous feature of TiO_2 and C, which indicates the C species can improve the specific surface area of the composite.

10.1002/cnma.202200075

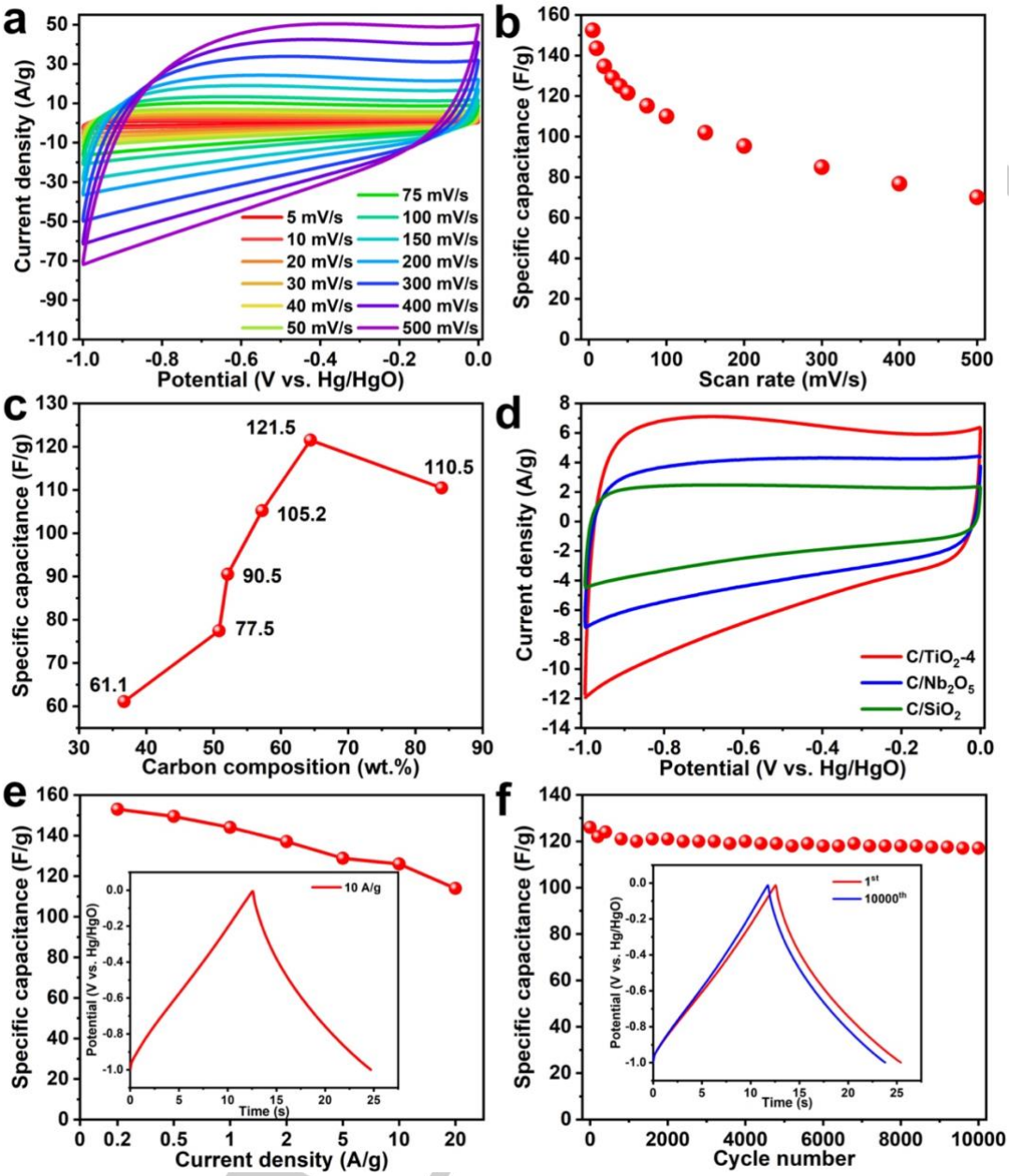

Figure 3. Supercapacitive performance of C/TiO_2-4. a and b). CV profiles and their corresponding specific gravimetric capacitances at different scan rates. c). Specific gravimetric capacitances of C/TiO_2-4 composites with different C compositions at 50 mV s^{-1}. d). CV profiles of three prepared C/oxides and pure porous C at 50 mV s^{-1}. e). Rate capability and the GCD curves at a current density of 10 A g^{-1} (inset). f). Long-term cyclic performance at a current density of 10 A g^{-1} and the initial and final GCD curves (inset).

With the consideration of the aforementioned unique chemical and structural features of C/TiO_2-4 composite, exploiting its supercapacitive property is of interest. As the cyclic voltammetry (CV) curves shown in Figure 3a, the typical quasi-rectangular profiles at different scan rates are observed, demonstrating the pure capacitive behavior of C/TiO_2-4. The calculated specific capacitances at scan rates of 5, 10, 20, 30, 40, 50, 75, 100, 150, 200, 300, 400 and 500 mV s^{-1} are 152.4, 143.5, 134.6, 129.1, 124.9, 121.5, 115.2, 110.0, 101.9, 95.3, 84.9, 76.8 and 70.1 F g^{-1} (Figure 3b), respectively, which reflects excellent capacitance retentions of 84.7%, 72.2% and 46.0% at 30, 100 and 500 mV s^{-1}. As presented in Figure 3c, to evaluate the effect of the C species in the prepared C/TiO_2-4 composite, a set of C/TiO_2 composites with different C compositions were ionothermally prepared and tested, revealing that the C/TiO_2-4 presents the optimized performance. Moreover, a set of machine learning studies was performed following previous literature via artificial neural network (ANN) model.[26] As shown in Table S1, the predicted electrochemical performance of C/TiO_2-4 is in line with the experimental results, illustrating the promising supercapacitive character of C/TiO_2-4 composite. Noticeably, comparing to the previously reported carbon-TiO_2 composites and

some other carbon-oxide composites (Table S2), the obtained C/TiO_2-4 indeed presents excellent supercapacitive performance, indicating the success of our proposed ionothermal synthesis strategy. Furthermore, to determine the influence of the C component in the C/TiO_2-4 on the supercapacitive performance, an electrochemically inactive C/SiO_2 composite baseline material with highly comparable surface area (435.0 m^2 g^{-1}) and C composition (60.1 wt.%) (Figure S16 and S18), was synthesized and tested *via* the identical method. As expected, as displayed in Figure S31a and S31b, the obtained capacitances of the prepared C/SiO_2 composite are significantly lower than those of C/TiO_2-4, which directly unveils that the mainly contribution of the capacitance of the C/TiO_2-4 is from the prepared anatase TiO_2 nanocrystallites, confirming the effectiveness of the proposed in-situ ionothermal synthesis of C/TiO_2-4 composite. Such promising electrochemical performance can be attributed to the highly porous structure of the prepared C/TiO_2-4 material and the potentially enhanced electrical conductivity of TiO_2 rooted from the self-doping of Ti^{3+},[4b, 27] further implying the advantages of ionothermal synthesis for the preparation of supercapacitor electrode materials. Additionally, the *in-situ* formed N-rich C species in the composite not only can improve the conductivity of composite electrode but also can react with electrolyte to generate more capacitance.[15]

To further demonstrate the versatility and practicality of the proposed in-situ ionothermal synthesis, different ILs and C/transition metal oxide composites were applied and prepared, respectively. On the one hand, with the consideration of the choice of IL, 1-(cyanomethyl)-3-propargylimidazolium bis(trifluoromethanesulfonyl)imide ([CNPIm][NTf_2]), as a nitril-contained IL with extremely high C yield was employed.[10a] As shown in Figure S19a, the [CNPIm][NTf_2]-based C/TiO_2 presents highly similar XRD pattern with the aforementioned [BMIm][NTf_2]-prepared C/TiO_2 material. The Rietveld refinement suggests that anatase TiO_2 presents lattice parameters of a = b = 3.793 Å, c = 9.491 Å and $\alpha = \beta = \gamma = 90$ ° with a unit cell volume of 136.5 $Å^3$, which also indicates an expanded lattice of the formed anatase TiO_2 (Figure S19b), implying the Ti^{3+} self-doping effect because of the appearance of the reduction of Ti^{4+} in the lattice. Furthermore, the grain size of the [CNPIm][NTf_2]-based TiO_2 estimated from Scherrer equation is around 7.1 nm. Additionally, as displayed in Figure S20 and S22, the specific surface area and C composition of the [CNPIm][NTf_2]-based C/TiO_2 are 412.6 m^2/g and 59.4 wt.%, which are comparable to those of the [BMIm][NTf_2]-prepared C/TiO_2. As shown in Figure S31c and S31d, the supercapactive performance at scan rates of 5, 10, 20, 30, 40, 50, 75, 100, 150, 200, 300, 400 and 500 mV s^{-1}, respectively is 136.8, 127.3, 120.3, 116.1, 113.1, 110.5, 106.3, 102.9, 93.6, 93.2, 85.7, 79.3 and 73.7 F g^{-1}. Thereby, the broadness of the choice of IL in this proposed ionothermal synthesis strategy is confirmed. On the other hand, to demonstrate the practicality of the proposed strategy with other metal oxides, a C/Nb_2O_5 composite was synthesized via $NbCl_5$ and [BMIm][NTf_2]. As shown in Figure S24, the XRD pattern of C/Nb_2O_5 match the standard diffraction pattern (ICDD 00-028-0317), implying the obtained Nb_2O_5 is in the hexagonal system with a space group of *PE*. Exhibited in Figure S25, the nitrogen adsorption isothermal of C/Nb_2O_5 is highly similar to that of C/TiO_2-4 (Figure S5), indicating a large specific surface area of 235.1 m^2/g with abundant micropores and mesopores. The TGA study suggests that C/Nb_2O_5 contains 62.1 wt.% of C material (Figure S27), which is also comparable to that of C/TiO_2. More interestingly, as displayed in Figure S31e and S31f, the CV test reveals the good supercapacitive performance of C/Nb_2O_5, which delivers high specific capacitances of 103.4, 95.5, 87.6, 82.9, 80.1, 77.6, 73.5, 70.3, 65.6, 62.1, 56.5, 52.6 and 49.1 F g^{-1} at scan rates of 5, 10, 20, 30, 40, 50, 75, 100, 150, 200, 300, 400 and 500 mV s^{-1}, respectively. Such results above reflect excellent capacitance retentions of 80.2%, 68.0% and 47.5% at 30, 100 and 500 mV s^{-1}, correspondingly. As exhibited in Figure 3d, although C/TiO_2-4, C/Nb_2O_5 and C/SiO_2 with the comparable C composition exhibit the typical quasi-rectangular CV profiles, C/TiO_2-4 indeed presents the best supercapacitive performance among the three prepared C/oxides, which is close to that of a [CNPIm][NTf_2]-pyrolyzed highly porous C with a large specific surface area of 835.5 m^2 g^{-1} (specific capacitances of 161.2, 150.7, 140.1,134.2, 129.9, 126.5, 120.7, 116.2, 109.5, 104.3, 96.0, 89.2 and 82.7 F g^{-1} at scan rates of 5, 10, 20, 30, 40, 50, 75, 100, 150, 200, 300, 400 and 500 mV s^{-1}, respectively), shown in Figure S29, S31g and S31h. Therefore, the versatility and practicality of the proposed ionothermal synthesis strategy for C/metal oxide composites are confirmed, which presents the broad choice of IL and metal oxide.

To further study the supercapacitive performance of the prepared C/TiO_2-4 composite, a series of galvanostatic charge/discharge (GCD) tests was conducted to characterize the rate capability and long-term cyclability. As shown in Figure 3e, desirable specific capacitances of 152.8, 149.5, 144.0, 137.1, 128.8, 126.0 and 114.0 F g^{-1} are achieved at current densities of 0.2, 0.5, 1, 2, 5, 10 and 20 A g^{-1}, respectively. The specific capacitance retention of C/TiO_2-4 composite electrode at 20 A g^{-1} is 75%, indicating promising rate capability. This superb rate capability is mainly attributed to its improved conductivity and porous structure, which benefit the electron transfer and electrolyte transportation. Noticeably, the GCD curves displayed in the inset and Figure S32 present triangular shape, implying the effect of electric double-layer capacitance, which is consistent with the CV study in Figure 3a above. The study of the long-term cyclability of C/TiO_2-4 was further conducted at a high current density of 10 A g^{-1} (Figure 3f). Impressively, the measured first and 10,000th specific capacitances are 126.0 and 117.1 F g^{-1}, corresponding to a good retention rate of 93% over 10,000 cycles. As Figure 3f inset shown, the initial and final GCD curves share same appearance, indicating the excellent electrochemical stability of the C/TiO_2-4 electrode. The aforementioned excellent rate capability and long-term cyclability from GCD studies further reveal the success of our proposed ionothermal synthesis strategy for nanoporous C/oxide composite.

Conclusion

In summary, nanoporous C/oxide composites were successfully prepared *via* a facile ionothermal synthesis approach, which simultaneously applies IL as the solvent, porous structure directing template and carbon source. This in-situ ionothermal synthesis enables the tunable porosity and carbon composition of the prepared C/TiO_2-4 composite. As a result, the obtained C/TiO_2-4 material with nanoporous feature exhibits excellent electrochemical performance as a supercapacitor electrode material, which is mainly attributed to the synergistic effects of the highly porous structure, the vast lone pairs of electrons on N

induced Lewis base effect, the abundant defects with high electrical conductivity of the amorphous C species and the Ti^{3+} self-doping enhanced electrical conductivity of TiO_2 nanocrystallites. Therefore, this work establishes a promising strategy for the preparation of highly porous carbon/transition metal oxide composite materials for task-specific applications, such as supercapacitors or lithium-ion batteries.

Experimental Section

In-situ ionothermal syntheses of carbon/oxides composites and highly porous carbon

Typically, 1 mL of titanium (IV) butoxide ($Ti(OBu)_4$), 1 mL of acetic acid and 0.1 mL of formic acid were dissolved in 0.5, 1, 2, 3, 4 or 5 mL of 1-butyl-3-methylimidazolium bis(trifluoromethylsulfonyl)imide ([BMIm][NTf_2]). After stirring the mixture for 30 min, the mixtures were gelled at 50 °C followed by pyrolysis at 600 °C for 4 h at a ramp of 2 °C/min in nitrogen atmosphere. The obtained composites were denoted as C/TiO_2-x (x=0.5 – 5), where x is the volume ratio of [Bmim][NTf2]/$Ti(OBu)_4$. Note: if precipitate formed in the liquid mixture, anhydrous methanol would be added.

To further demonstrate the versatility of the in-situ ionothermal synthesis strategy, a nitrile-contained IL with high carbon yield was used to prepare C/TiO_2 composite. Particularly, 1 mL of titanium (IV) butoxide ($Ti(OBu)_4$), 1 mL of acetic acid and 0.1 mL of formic acid were dissolved in 0.5 mL of 1-(cyanomethyl)-3-propargylimidazolium bis(trifluoromethanesulfonyl)imide ([CNPIm][NTf_2]). After stirred the mixture for 30 min, the mixtures were gelled at 50 °C followed by pyrolysis at 600 °C for 4 h at a ramp of 2 °C/min in nitrogen atmosphere. Additionally, a C/Nb_2O_5 composite was also prepared. 0.76 g of $NbCl_5$, 1 mL of acetic acid and 0.1 mL of formic acid were dissolved in 4 mL of [BMIm][NTf_2]. After stirred the mixture for 30 min, the mixtures were gelled at 50 °C followed by pyrolysis at 600 °C for 4 h at a ramp of 2 °C/min in nitrogen atmosphere. Note: if precipitate formed in the liquid mixture, anhydrous methanol would be added. To estimate the potential capacitive contribution of the formed C material in the C/TiO_2, a C/SiO_2 composite with comparable C wt.% and surface area was synthesized. Typically, 2 mL of tetramethyl orthosilicate and 1 mL of formic acid were dissolved in 2 mL of [BMIm][NTf_2]. After stirring the mixture for 30 min, the mixtures were gelled at 50 °C followed by pyrolysis at 600 °C for 4 h at a ramp of 2 °C/min in nitrogen atmosphere. Moreover, a pure porous C material was further prepared via pyrolysis of [CNPIm][NTf_2] at 600 °C for 4 h at a ramp of 2 °C/min in nitrogen atmosphere.

Typical characterizations

Powder X-rays diffraction (XRD) patterns were recorded on a Kα Cu-coupled diffractometer (Panalytical Empyrean) at an operation voltage of 45 kV and a current of 40 mA, and the obtained XRD patterns were analyzed by HighScore Plus from Malvern Panalytical. Fourier-transform infrared spectroscopy (FTIR) tests were performed on a Thermo Scientific™ Nicolet™ iS50 FTIR spectrometer. Raman data were collected from a Raman model HORIBA microscope with a solid-state 532-nm excitation lase. X-ray photoelectron spectra (XPS) were obtained on a Thermo Scientific X-ray photoelectron spectrometer with a monochromated Al Kα (1486. 6 eV) X-ray source focused to a 400-micron spot under a pressure below 1×10^{-7} mbar, and the energy calibration and deconvolution of XPS peaks were analyzed by CasaXPS (Casa Software Ltd). N_2 isothermal adsorption tests were carried on a Micromeritics Gemini VII adsorption analyzer. Scanning electron microscope (SEM) analysis was carried out on a Carl Zeiss Auriga 40 SEM microscope, and SEM energy dispersive X-ray (EDX) element mapping was conducted on a Carl Zeiss EVO MA15. Transmission electron microscope (TEM) images were recorded on a Nion UltraSTEM 200 at 200 kV. Thermogravimetric analysis (TGA) studies were performed on a Q-50 TGA analyzer from TA Instruments in air atmosphere at a ramp of 20 °C/min.

Electrochemical characterization

Supercapacitor cyclic voltammetry (CV) and galvanostatic charge/discharge (GCD) studies were conducted on a CHI604B electrochemical analyzer in 1 M KOH. The typical three-electrode cell was composed of a carbon/oxide coated glassy carbon (GC) working electrode, a Pt counter electrode and a Hg/HgO reference electrode. To prepare the working electrode, 1.4 mg of carbon/oxide was sonicated and dispersed in a 1 mL ethanol–water mixture (1:1) for 1 h. Afterwards, 10 µL of the dispersion was drop-casted onto a GC electrode with 10 µL of 0.05 wt.% Nafion binder solution. After air-drying the working electrode at room temperature, CV and GCD tests were performed.

The calculation of the specific capacitance was based on the CV curves *via* using the following equation below,

$$C_m = \frac{\int I dU}{2mv\Delta U},$$

where C_m, I, m, v and ΔU refer to the specific capacitance (F g^{-1}), the measured current (A), the active material mass loading on the working electrode (g), the scan rate (V s^{-1}) and the potential window (V), respectively.

The calculation of the specific capacitance of GCD was based on the following equation below,

$$C_m = \frac{I\Delta t}{m\Delta U},$$

where C_m, I, Δt, m and ΔU refer to the specific capacitance (F g^{-1}), the measured current (A), the discharge time (s), the active material mass loading on the working electrode (g) and the potential window (V), respectively.

Machine learning

Artificial neural network (ANN) model was applied to study the overall specific capacitances of the prepared C/TiO_2 composites with different C compositions based on the surface areas of micropores and mesopores, following the previous literature.[26]

Acknowledgements

The research at Oak Ridge National Laboratory and the University of Tennessee at Knoxville was supported by the U.S. Department of Energy's Office of Science, Office of Basic Energy Science, Division of Materials Sciences Engineering under contract No. DE-AC05-00OR22725. The authors thanks Dr. Guang Yang and Dr. Jagjit Nanda for the experimental support on Raman spectrometer. This manuscript has been authored by UT-Battelle, LLC under contract No. DE-AC05-00OR22725 with the U.S. Department of Energy.

Conflict of Interest

The authors declare no conflict of interest.

Keywords: ionothermal synthesis • ionic liquid • TiO_2 • porous material • supercapacitor

[1] G. Wang, L. Zhang, J. Zhang, *Chem. Soc. Rev.* **2012**, *41*, 797-828.
[2] P. Simon, Y. Gogotsi, *Nat. Mater.* **2008**, *7*, 845-854.
[3] a) M. S. Kim, T.-W. Lee, J. H. Park, *J. Electrochem. Soc.* **2009**, *156*, A584; b) M. Zhou, A. M. Glushenkov, O. Kartachova, Y. Li, Y. Chen, *J. Electrochem. Soc.* **2015**, *162*, A5065; c) L. Zhang, Q. Song, C. Wang, X. Liu, X. Jiang, J. Gong, *J. Nanomater.* **2020**, *2020*, 6642236.
[4] a) C. Dette, M. A. Pérez-Osorio, C. S. Kley, P. Punke, C. E. Patrick, P. Jacobson, F. Giustino, S. J. Jung, K. Kern, *Nano Lett.* **2014**, *14*, 6533-6538; b) A. Elmouwahidi, E. Bailón-García, J. Castelo-Quibén, A. F. Pérez-Cadenas, F. J. Maldonado-Hódar, F. Carrasco-Marín, *J. Mater. Chem. A* **2018**, *6*, 633-644.
[5] a) M. Zhi, C. Xiang, J. Li, M. Li, N. Wu, *Nanoscale* **2013**, *5*, 72-88; b) T. Lu, Y. Zhang, H. Li, L. Pan, Y. Li, Z. Sun, *Electrochim. Acta* **2010**, *55*, 4170-4173; c) X. Sun, M. Xie, G. Wang, H. Sun, A. S. Cavanagh, J. J. Travis, S. M. George, J. Lian, *J. Electrochem. Soc.* **2012**, *159*, A364.
[6] R. Górniak, S. Lamperski, *J. Phys. Chem. C* **2014**, *118*, 3156-3161.
[7] a) Z. Ma, J. Yu, S. Dai, *Adv. Mater.* **2010**, *22*, 261-285; b) R. D. Rogers, *Nature* **2007**, *447*, 917-918.
[8] a) M. Armand, F. Endres, D. R. MacFarlane, H. Ohno, B. Scrosati, *Nat. Mater.* **2009**, *8*, 621-629; b) R. D. Rogers, K. R. Seddon, *Science* **2003**, *302*, 792.
[9] a) R. Tao, G. Yang, E. C. Self, J. Liang, J. R. Dunlap, S. Men, C.-L. Do-Thanh, J. Liu, Y. Zhang, S. Zhao, H. Lyu, A. P. Sokolov, J. Nanda, X.-G. Sun, S. Dai, *Small* **2020**, *16*, 2001884; b) P. Zhang, H. Lu, Y. Zhou, L. Zhang, Z. Wu, S. Yang, H. Shi, Q. Zhu, Y. Chen, S. Dai, *Nat. Commun.* **2015**, *6*, 8446; c) B. Wang, J. Di, P. Zhang, J. Xia, S. Dai, H. Li, *Appl. Catal. B* **2017**, *206*, 127-135; d) X. Zhu, P. C. Hillesheim, S. M. Mahurin, C. Wang, C. Tian, S. Brown, H. Luo, G. M. Veith, K. S. Han, E. W. Hagaman, H. Liu, S. Dai, *ChemSusChem* **2012**, *5*, 1912-1917; e) S. Zhou, Z. Ma, G. A. Baker, A. J. Rondinone, Q. Zhu, H. Luo, Z. Wu, S. Dai, *Langmuir* **2009**, *25*, 7229-7233; f) X. Cui, Q. Yang, Y. Xiong, Z. Bao, H. Xing, S. Dai, *Chem. Commun.* **2017**, *53*, 4915-4918; g) Q. Yang, Z. Zhang, X.-G. Sun, Y.-S. Hu, H. Xing, S. Dai, *Chem. Soc. Rev.* **2018**, *47*, 2020-2064.
[10] a) J. S. Lee, X. Wang, H. Luo, G. A. Baker, S. Dai, *J. Am. Chem. Soc.* **2009**, *131*, 4596-4597; b) X. Wang, S. Dai, *Angew. Chem. Int. Ed.* **2010**, *49*, 6664-6668.
[11] a) S. Dai, Y. H. Ju, H. J. Gao, J. S. Lin, S. J. Pennycook, C. E. Barnes, *Chem. Commun.* **2000**, 243-244; b) Z. Ma, J. Yu, S. Dai, *Adv. Mater.* **2010**, *22*, 261-285; c) A. Vioux, *Chem. Mater.* **1997**, *9*, 2292-2299; d) Y. Zhou, J. H. Schattka, M. Antonietti, *Nano Lett.* **2004**, *4*, 477-481.
[12] T. E. Weirich, M. Winterer, S. Seifried, J. Mayer, *Acta Crystallographica Section A: Foundations of Crystallography* **2002**, *58*, 308-315.
[13] R. D. Shannon, *Acta Crystallogr. Sec. A* **1976**, *32*, 751-767.
[14] L. Yang, P. W. May, L. Yin, J. A. Smith, K. N. Rosser, *Journal of Nanoparticle Research* **2007**, *9*, 1181-1185.
[15] a) F. Sun, H. Wu, X. Liu, F. Liu, H. Zhou, J. Gao, Y. Lu, *Nano Res.* **2016**, *9*, 3209-3221; b) B. B. Garcia, S. L. Candelaria, G. Cao, *J. Mater. Sci.* **2012**, *47*, 5996-6004.
[16] W. Zhang, Y. He, M. Zhang, Z. Yin, Q. Chen, *J. Phys. D: Appl. Phys.* **2000**, *33*, 912.
[17] S. Chen, R. Tao, J. Tu, P. Guo, G. Yang, W. Wang, J. Liang, S.-Y. Lu, *Adv. Funct. Mater.* **2021**, *31*, 2101199.
[18] Y. Chen, Z. Li, S. Shi, C. Song, Z. Jiang, X. Cui, *J. Mater. Sci.: Mater. Electron.* **2017**, *28*, 9206-9220.
[19] aH. Song, Y.-T. Kim, *Chem. Commun.* **2015**, *51*, 9849-9852; bS. Lou, X. Cheng, Y. Zhao, A. Lushington, J. Gao, Q. Li, P. Zuo, B. Wang, Y. Gao, Y. Ma, C. Du, G. Yin, X. Sun, *Nano Energy* **2017**, *34*, 15-25.
[20] K. Li, Z. Huang, X. Zeng, B. Huang, S. Gao, J. Lu, *ACS Appl. Mater. Interfaces* **2017**, *9 13*, 11577-11586.
[21] T. K. Rahul, M. Mohan, N. Sandhyarani, *ACS Sustainable Chem. Eng.* **2018**, *6*, 3049-3059.
[22] X. Wang, G. Shen, *Nano Energy* **2015**, *15*, 104-115.
[23] C. Xu, Q. Han, Y. Zhao, L. Wang, Y. Li, L. Qu, *J. Mater. Chem. A* **2015**, *3*, 1841-1846.
[24] Y. Li, P. Li, J. Wang, Y. Yang, W. Yao, Z. Wei, J. Wu, X. Yan, X. Xu, Y. Liu, Y. Zhu, *Appl. Catal. B: Environ.* **2018**, *225*, 519-529.
[25] a) Y. Qin, X. Han, S. Gadipelli, J. Guo, S. Wu, L. Kang, J. Callison, Z. Guo, *J. Mater. Chem. A* **2019**, *7*, 6543-6551; b) M.-S. Lee, M. Park, H. Y. Kim, S.-J. Park, *Sci. Rep.* **2016**, *6*, 23224; c) F. Ma, S. Ding, H. Ren, Y. Liu, *RSC Adv.* **2019**, *9*, 2474-2483.
[26] a) M. Zhou, A. Vassallo, J. Wu, *ACS Appl. Energy Mater.* **2020**, *3*, 5993-6000; b) T. Wang, R. L. Sacci, J. Liang, C.-L. Do-Thanh, J. Fan, H. Chen, Y. Sun, B. P. Thapaliya, S. M. Mahurin, M. Zhou, J. Wu, S. W. Donne, S. Dai, *J. Electrochem. Soc.* **2021**, *168*, 060530; c) M. Zhou, A. Gallegos, K. Liu, S. Dai, J. Wu, *Carbon* **2020**, *157*, 147-152.
[27] T. Jin, X. Sang, R. R. Unocic, R. T. Kinch, X. Liu, J. Hu, H. Liu, S. Dai, *Adv. Mater.* **2018**, *30*, 1707512.

10.1002/cnma.202200075

WILEY-VCH

RESEARCH ARTICLE

Entry for the Table of Contents

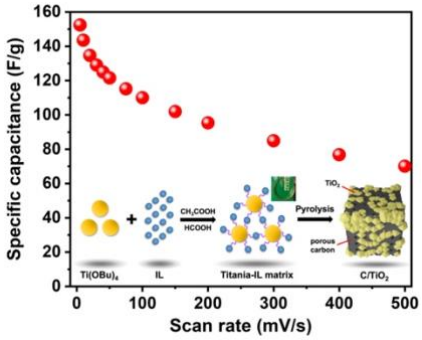

This work describes a facile in-situ ionothermal synthesis strategy for highly nanoporous carbon/oxides composites, which applies ionic liquids as the solvents, templating agents and carbon sources (spatially confined pyrolysis), achieving nano feature, porosity and high carbon yield. Therefore, the prepared carbon/titanium oxide composite delivers an promising electrochemical performance as the supercapacitor electrodes.